RADIO SCIENCE Journal of Research NBS/USNC-URSI
Vol. 68D, No. 8, August 1964

Broadband Radio-Star Scintillations, Part I. Observations

D. G. Singleton [1]

Contribution From the High Altitude Observatory, University of Colorado, Boulder, Colo.

(Received March 3, 1964; revised March 26, 1964)

Twelve months' observations of the scintillations of Cassiopeia A made with a swept-frequency interferometer operating in the frequency range 7.6 to 41 Mc/s are examined statistically. The scintillations, which commonly have bandwidths of 2:1 and larger, are occasionally associated with apparent shifts in the position of the source. Two types of position shift patterns are observed. These are mirror images of each other and occur during different periods of sidereal time. The broadband scintillations also occasionally exhibit dispersion. This effect is most marked before 0900 hours local sidereal time and after 0200 hours local time. The overall occurrence picture of the broadband scintillations is much as reported by other workers for scintillations observed at discrete frequencies. Broadband scintillation occurrence is found to correlate positively with the occurrence of spread-*F*. The focus frequency of those scintillations which exhibit position shifts is found to depend, in a simple way, on the parameters of the associated spread-*F* configuration. Increasing magnetic activity, which has little effect on the occurrence of the scintillations, is found to be associated with a decrease in the quasi-period of groups of scintillations. The interpretation of these observations will appear in part II of the series.

1. Introduction

Throughout the last decade much has been learned of the nature of ionospheric irregularities by means of radio astronomical studies of the upper atmosphere [Booker, 1958; Aarons, 1963]. Both radio stars and satellites have been used as sources of radio waves in these studies, the majority of which have been carried out at discrete frequencies. Most of the observations have been interpreted in terms of ionization irregularities in the *F*-region, statistical methods based on the theory of diffraction at an irregular screen being used.

In 1956 Wild and Roberts reported the first study of the dynamic spectra of radio-star scintillations in the frequency range 40 to 70 Mc/s. They were forced to interpret their results in terms of a mechanism other than diffraction at an irregular screen. They suggested that many features of their observations could only be explained in terms of the ionospheric irregularities behaving as large lenses and/or prisms refracting the incoming radio waves in an irregular manner. This suggestion has been taken up recently by Warwick [1964], in order to explain some features of the broadband scintillations observed with the Boulder spectrointerferometer. The purpose of part I of this communication is to display the whole range of scintillation phenomena observed within the 7.6 to 41 Mc/s frequency range of the Boulder spectrointerferometer and to discuss some of the statistical properties of the different phenomena. Part II will investigate the extent to which the refractive properties of ionospheric irregularities can be invoked to explain these observations.

[1] On sabbatical leave from the Physics Department, University of Queensland, Australia.

2. Description of the Observations

The observations of Cassiopeia A described here were made with a spectrographic interferometer operating within the frequency range 7.6 to 41 Mc/s at Boulder, Colo. (40.1° N, 105.3° W). Observations of the Sun and the planet Jupiter with this instrument have been described elsewhere [Boischot et al., 1960; Warwick, 1961 and 1963] while a description of the swept-frequency receiver used is in press [Lee and Warwick, 1964]. The facsimile method of recording allows the frequency and time structure of the interferometer fringes excited by the emissions of Cassiopeia A to be displayed on a frequency-time plot. The smoothly changing position of the source associated with its diurnal motion produces, in the presence of an undisturbed ionosphere, a regular drift of the fringes across the frequency scale as time proceeds. When the ionosphere is disturbed this smooth pattern is punctuated with apparent shifts in the position of the source and/or variations in the intensity of the source. These are the scintillations which will be discussed here.

2.1. Broadband Nature of the Scintillations

The most striking feature of the scintillations observed by the spectrointerferometer is their broad bandwidth. The spectrograph in the middle of figure 1 illustrates this. Most of the scintillations on this figure have bandwidths of 2:1 while that at 0508 UT has a bandwidth of nearly 3:1. While scintillations with bandwidths of 2:1 to 3:1 are common, it is very rarely that scintillations with bandwidths of more than 4:1 are encountered. This

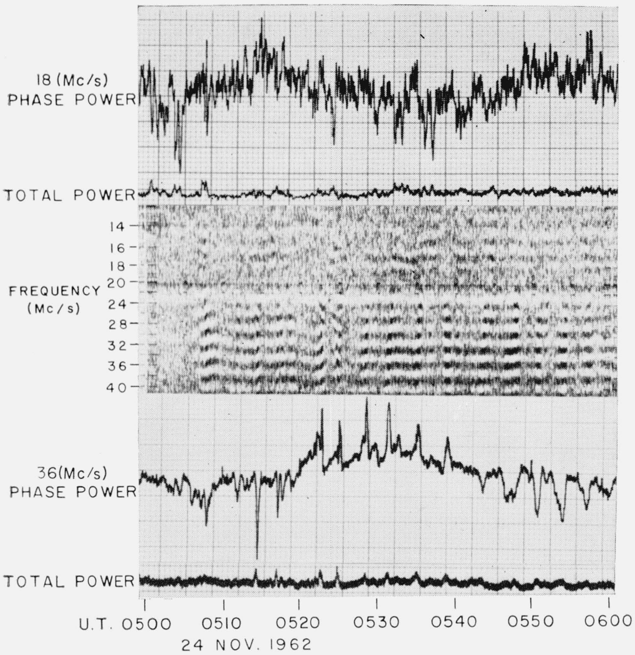

FIGURE 1. *A spectrogram and the corresponding records of the 18 and 36 Mc/s fixed-frequency interferometers reproduced so that they are in synchronism.*

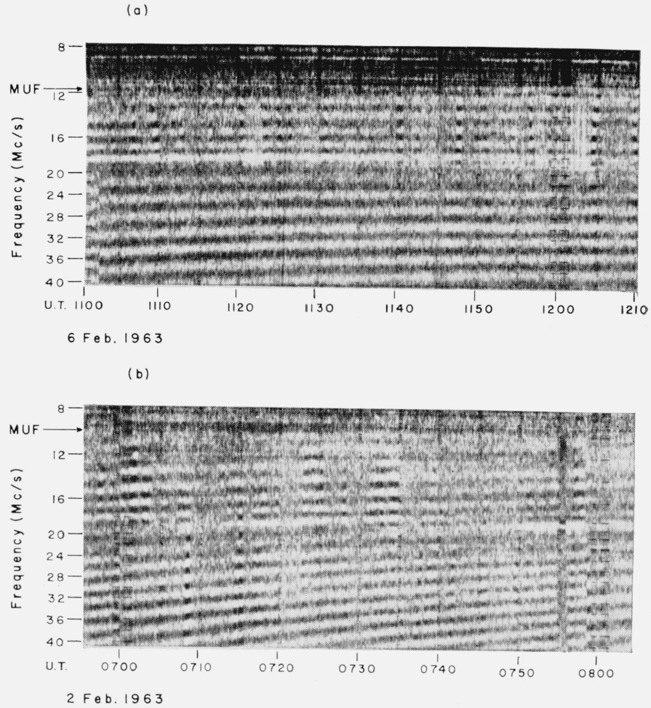

FIGURE 2. *Two spectrograms showing (a) scintillations which exist only at low frequencies and (b) scintillations which exist in the low frequency part of the record or in the high frequency part.*

feature, first noted by Wild and Roberts [1956] and subsequently by Warwick [1964] would seem to be in contradiction with comparisons of scintillations made simultaneously at two or more fixed frequencies [Bolton and Stanley, 1948; Smith, 1950; Burrows and Little, 1952; Chivers, 1960] which suggest that correlation over frequency ranges as high as 2:1 are unlikely. Detailed examination of figure 1, however, shows that this is not necessarily the case. Figure 1 contains, besides the spectrograph, 36 and 18 Mc/s fixed-frequency interferometer records of Cassiopeia A made at Boulder. The time scales of the records have been adjusted in the reproduction so that they are in synchronism. It will be noted that of the scintillations detected by the fixed-frequency equipments only those of large amplitude are obvious on the spectrograph. This is partly due to a lack of contrast on the part of the smaller fluctuations and partly due to a lack of frequency integration. Thus while numerous scintillations with 2:1 bandwidths appear on the spectrograph in the 20 to 40 Mc/s range, the fixed-frequency records at 18 Mc/s and 36 Mc/s do not show high correlation.

The broadband scintillations are found to be centered anywhere within the frequency range 7.6 to 41 Mc/s. The examples shown in figure 1 happen to be centered about 30 Mc/s. In figure 2a on the other hand, the central frequency of the scintillations is of the order of 15 Mc/s. Figure 2b shows a period in which the broadband scintillations are sometimes on a low frequency (about 15 Mc/s) and sometimes on a higher frequency (about 28 Mc/s).

Quite often the possibility of observing scintillations in the lower octaves is precluded by interference from communication stations. In the two examples of figure 2, the maximum usable frequency of the section of the ionosphere being examined and the communication station density in the appropriate part of the earth's surface are such that the interference is limited to frequencies below about 10 Mc/s (referred to as the MUFE) and scintillations only above this frequency are readily observable. On many occasions, however, the MUFE is of the order of 20 Mc/s and consequently it is not possible to obtain realistic figures on the relative occurrence of the central frequency of the broadband scintillations within the frequency range of the spectrointerferometer. This point will be discussed further in section 3.4.

2.2. Position Shifts

The spectrointerferometer, besides being able to detect scintillations as changes in amplitude, is also capable of detecting any shifts in the apparent position of the source associated with the scintillations. Such position shifts give rise to fringe slopes within the duration of a scintillation which differ from those immediately before and after the scintillation.

Many of the broadband scintillations observed show no measurable shift in position. Scintillations with this characteristic are referred to as N type scintillations in what follows. A schematic representation of this type of scintillation is shown in figure 3a while several of these scintillations (labeled A) are shown in the spectrograms reproduced in figure 4.

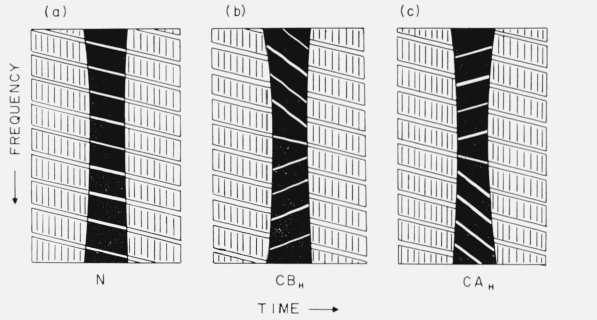

FIGURE 3. *A schematic representation of position shift configurations within a scintillation.*

(a) represents classification N, (b) classification CB_H and (c) classification CA_H.

The scintillations which exhibit position shifts fall into two main categories, the pattern of fringe shifts for one category being the mirror image of that for the other. In the first of these categories, designated CB_H, the high-frequency fringes, at the beginning of the scintillation, each jump sharply to a slightly higher frequency than that dictated by the source's diurnal motion. This initial increase in frequency for each fringe order is followed by a uniform decrease in frequency during the scintillation until, at the end of the scintillation, the frequency for each order is lower than that required by the undisturbed direction of the source. At the lower frequencies the reverse pattern of change of frequency occurs for each order during the scintillation. At some intermediate frequency the fringe slope within the scintillation is the same as the normal slope associated with the diurnal motion of the source. This phenomenon is shown schematically in figure 3b, while examples of this category appear (labeled B) in figure 4. Scintillations conforming to a pattern of fringe shifts which is the mirror image of the type CB_H just described are designated CA_H. The CB_H scintillations invariably involve larger shifts in the apparent position of the source than CA_H scintillations. Figure 3c is a schematic representation of the CA_H type of fringe pattern, while actual examples (labeled C) are displayed in figure 4.

The CB_H and CA_H scintillation categories, besides having the distinctive fringe patterns described above, also often display a duration which is frequency dependent. As frequency is increased the scintillation narrows slightly in the horizontal (time) direction in the vicinity of the fringe slope changeover, increasing again at the higher frequencies. This effect is illustrated schematically in figures 3b and 3c and again in the cases labeled B and C in the spectrograph of figure 4.

While most scintillations whose fringe slopes depart from that expected in terms of the diurnal motion of the source exhibit the fringe patterns described as CB_H and CA_H above, there are a few in which the changeover in fringe slope at some intermediate frequency does not occur. These have been designated S_B or S_A depending on whether the fringes within the scintillation commence below or above

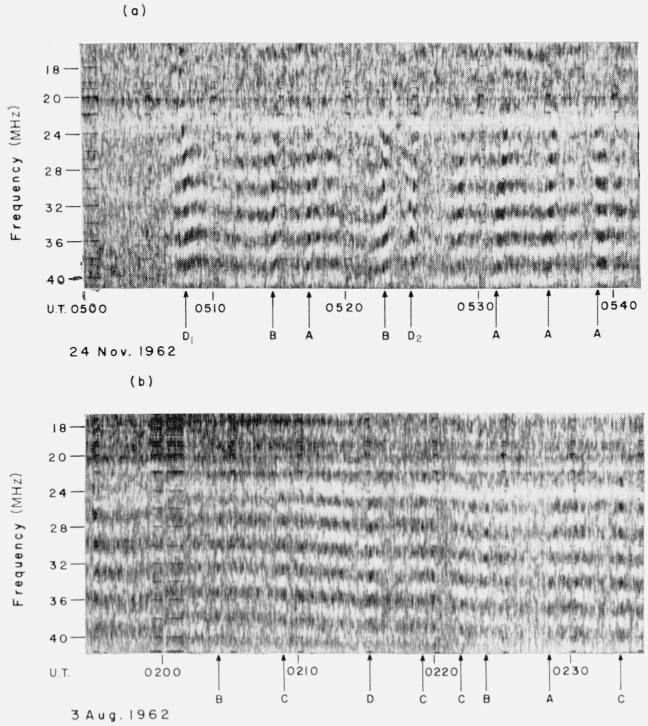

FIGURE 4. *Two spectrograms showing examples of the various position shift classifications.*

Those scintillations labeled A correspond to classification N, those labeled B to classification CB_H, those labeled C to classification CA_H, those labeled D to classification S_B and those labeled D_2 to classification S_A.

the frequency corresponding to the diurnal motion of the source for each fringe order. Examples of S_B (labeled D_1) and S_A (labeled D_2) are to be found in figure 4. Invariably these scintillations extend to 41 Mc/s or the MUFE and give every indication of continuing beyond the effective recording range. It is probable, therefore, that they represent the low frequency or high frequency parts of one of the more common CB_H or CA_H events in which the changeover frequency is outside the observable range. The low frequency part of CB_H or the high frequency part of CA_H would constitute the S_A event, while the high frequency part of CB_H on the low frequency part of CA_H would be classified as S_B.

2.3. Dispersion

Most of the broadband scintillations displayed in the spectrograms of figures 1, 2, and 4 are normal to the time axis. That is, in each of these cases, the scintillation occurs at much the same time for all the frequencies involved. While this represents the usual behavior of the broadband scintillations, some scintillations do not conform to this picture. For these there is a progressive shift of the time of the scintillation as the frequency is changed. In this effect, which is strongly suggestive of dispersion, the high frequencies may precede the low frequencies or vice versa. The time-frequency relationship may be such that the scintillation takes the form of a uniform straight strip inclined to the time axis or there may be considerable curvature involved.

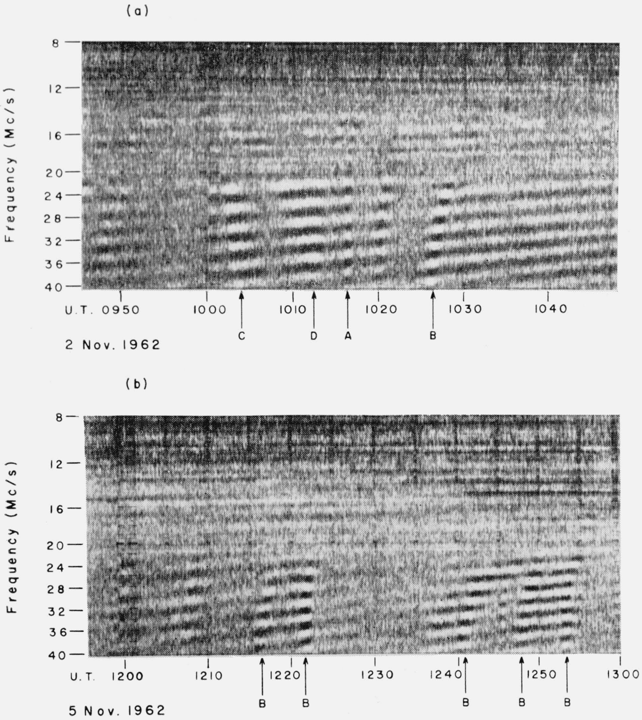

FIGURE 5. *Two spectrograms showing examples of the various dispersion classifications.*

Those scintillations labeled A correspond to classification NC–N/U, those labeled B to classification CS–T_L/U, that labeled C to classification CS–T_H/U and that labeled D to classification NC–T_H/L_L.

The scintillations have been classified according to their dispersion as well as in terms of any position shifts they may reveal. The classification, which is self-explanatory, is as follows:

- NC–N/U —no curvature, no dispersion, uniform width;
- NC–T_L/U—no curvature, sloping towards low frequencies as time progresses, uniform width;
- NC–T_H/U—no curvature, sloping towards high frequencies as time progresses, uniform width;
- CS–T_L/U —simple curvature, sloping towards low frequencies as time progresses, uniform width;
- CS–T_H/U —simple curvature, sloping towards high frequencies as time progresses, uniform width.

On a few occasions the width of the scintillation is much larger at its high frequency end or its low frequency end than elsewhere. On these occasions the U in the above classification is replaced by L_H (large at high frequencies) or L_L (large at low frequencies).

Some examples of these dispersive effects are displayed in the spectrographs of figure 5. Those labeled A are examples of the NC–N/U classification, those labeled B of the CS–T_L/U classification, those labeled C of the CS–T_H/U classification, and those labeled D of the NC–T_H/L_L classification.

On a very few occasions the low frequency end of a scintillation may appear to split in two taking on a forked configuration. This effect has been described in detail by Warwick [1964]. Scintillations with this feature have been classified dispersion-wise under CC–F (curvature complex, forked). The scintillation labeled D_2 on figure 4a is an example of this effect.

2.4. Relative Occurrence of the Various Classifications

Twelve months records (April 1962 to March 1963 inclusive) have been examined so as to determine the relative occurrence of the various position shift and dispersion classifications described in section 2.2 and 2.3. Each record was divided into half-hour periods of local and local sidereal time. Depending on the nature of the scintillations observed, one or more of both the position shift and dispersion classifications were allotted to each of these periods. By making use of this method of counting, the relative occurrence of each of the effects was found. The results are tabulated in tables 1 and 2. Each of the percentages quoted is the percentage of the total number of half-hour periods in which scintillations with the feature in question were observed.

TABLE 1. *Relative occurrence of the various position shift classifications of scintillations*

Classification	N	CB_H	CA_H	S_B	S_A
Percentage	91.8	11.9	6.8	1.7	0.6

Table 1 shows that the majority of scintillations are not associated with detectable shifts in the position of the source. Of those which exhibit position shifts, the CB_H variety is the most common, occurring about twice as frequently as CA_H. The S_B and S_A types occur infrequently.

TABLE 2. *Relative occurrence of the various dispersion classifications of scintillations*

Classification Percentage	NC–N/U 88.3		NC–N/L_H 0.2		NC–N/L_L 0.1	
Classification Percentage	NC–T_L/U 5.7	NC–T_H/U 1.5	NC–T_L/LH 0.9	NC–T_H/L_H 0.3	NC–T_L/L_L 0	NC–T_H/L_L 0.4
Classification Percentage	CS–T_L/U 3.8	CS–T_H/U 2.0	CS–T_L/L_H 2.0	CS–T_H/L_H 1.3	CS–T_L/L_L 0.6	CS–T_H/L_L 0.8
Classification Percentage	CC–F 0.6					

Table 2 reveals that most scintillations are free from dispersion. When dispersion does occur it results in the low frequencies being delayed relative to the high about three times as often as the reverse effect. Table 2 also shows that the great majority of scintillations are more or less uniform in duration across their bandwidth. The fork phenomenon is found to occur very infrequently.

3. Temporal Variations

As mentioned in section 2 the spectrointerferometer is used to observe the Sun and the planet Jupiter as well as Cassiopeia A. The outcome of the time sharing which results from this is that scintillation observations are not available for all local times nor for all sidereal times. The ranges of local times and sidereal times during which Cassiopeia A was observed during the period 1 April 1962 to 31 March 1963 are shown in figures 6a and 6b. The observations are limited to the night hours (1800 to 0600 hr local solar time) and 6 hr on either side of the source's lower culmination. Figure 7a also shows that most of the observations were made in the months of November through May.

3.1. Total Occurrence

Figures 6c, 6d, and 7b illustrate how the total occurrence of scintillations varies with local time, sidereal time and month of the year. The local time variation (fig. 6c) has a rather broad maximum centered on 0100 while figure 7b shows that there is little seasonal variation. Both these results are consistent with the findings of previous workers [e.g., Booker, 1958]. Figure 6d illustrates the rather interesting sidereal time variation. This shows some signs of being symmetrical about lower culmination. The distribution appears to peak some 2 to 3 hr on either side of the lower culmination, there being a shallow minimum at the time of lower culmination.

3.2. Position Shifts

Figure 8 displays the local time and sidereal time variations of the three main position shift categories of scintillations viz, N, CB_H, and CA_H. It appears that while the three categories are generally equally likely at any local time, CB_H and CA_H are markedly dependent on sidereal time and N less so. The CB_H and CA_H sidereal time variations are suggestive of some mechanism which changes from one state to another on the order of an hour after lower culmination.

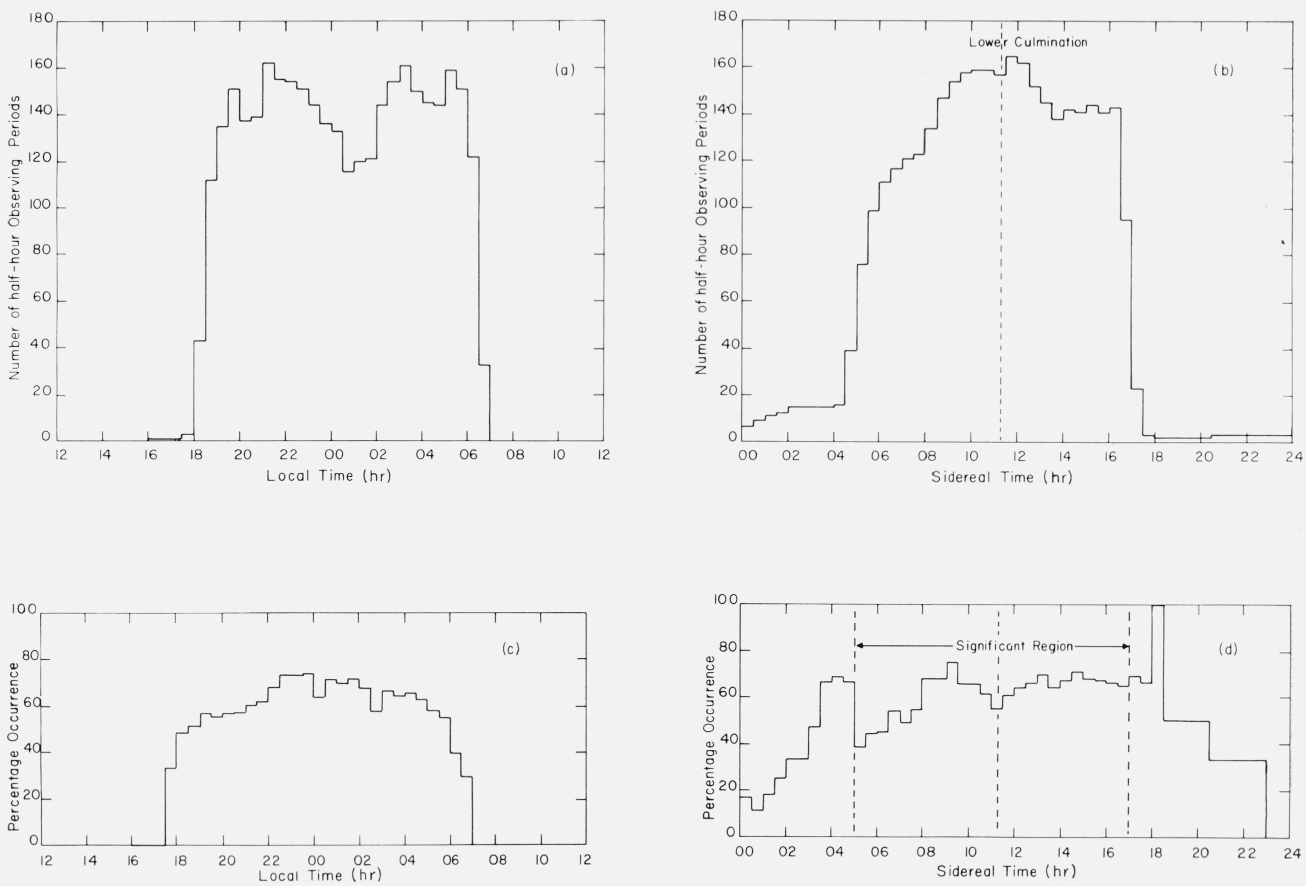

FIGURE 6. *Histograms of the number of half-hour observing periods versus (a) local time and (b) sidereal time and histograms of the percentage occurrence of scintillations versus (c) local time and (b) sidereal time.*

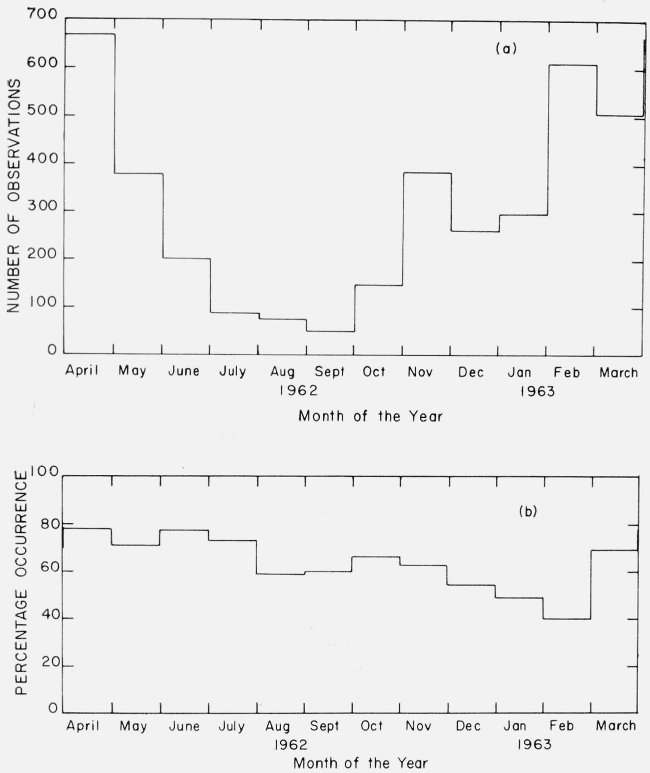

FIGURE 7. *Histograms of the number of half-hour observing periods versus month of the year (a) and the percentage occurrence of scintillations versus month of the year (b).*

It is perhaps important to establish that the apparently complementary sidereal time variations of CB_H and CA_H type scintillations are real and independent of other factors, in particular, local time. Close examination of figures 8c and 8e suggests that the CB_H and CA_H variations are possibly complementary especially in the period 0200 to 0700 hr. This raises some element of doubt as to the reality of the sidereal time distributions (figs. 8d and 8g). Any such doubt can, however, be eliminated by an examination of figures 9 and 10. Here the occurrences of CB_H (fig. 9) and CA_H (fig. 10) have been plotted on local time versus sidereal time plots as full lines. The broken lines enclose the period in which observations were made. It is immediately obvious that independently of local time the CB_H condition appears predominantly before 1200 hr sidereal time whereas the CA_H condition appears predominantly after 1200 hr. The sidereal time distributions of the CB_H and CA_H conditions are, therefore, judged to be independent of local time.

3.3. Dispersion

For the purpose of studying the temporal variations of the dispersion effects, scintillations which fall into the classifications NC–T_L/U and CS–T_L/U have been lumped together as have those which fall into the classifications NC–T_H/U and CS–T_H/U. That is, the scintillations have not been separated according to the extent of their curvature in the time-frequency domain but rather according to the direction of their general slope across this domain.

Figures 11a and 11b show the local time and sidereal time variations of those scintillations which have no dispersion (N). Figures 11c and 11d show these variations for scintillations whose dispersion is such that they lean towards the lower frequencies as time proceeds (NC–T_L/U and CS–T_L/U), while figures 11e and 11f are the temporal variations for scintillations whose dispersion is such that they lean towards the higher frequencies as time proceeds (NC–T_H/U and CS–T_H/U). The sidereal time variations show best the complementary nature of the scintillations which possess considerable dispersion and those which do not. Scintillations frequently have considerable dispersion before 0900 hr sidereal time and little between this time and 1600 hr when observations cease. The complementary nature of the occurrence of scintillations with and without dispersion is also evident, though less so, in the local time variations. Dispersion occurs more frequently after 0200 hr than before. To sum up, it appears that the mechanism giving rise to dispersion occurs more frequently for sidereal times earlier than 0900 hr and local times later than 0200 hr.

3.4. Scintillations at Low Frequencies

For a large part of the available observing time the MUFE was sufficiently high as to preclude the possibility of observing scintillations whose maximum frequency is less than 20 Mc/s. The occurrence figures quoted hitherto are thus largely dependent on scintillations which appear in the higher octaves. It is of interest, therefore, to examine the statistics of those scintillations which are observed in the lower octaves.

Figure 12 is a graphic illustration of the effect the MUFE has on the ability to see low-frequency scintillations. A value of the MUFE for each hour was obtained from the records and these data were used to construct figure 12a. This is a series of histograms for each month in which the number of hour observing periods is plotted against the MUFE values. The change of MUFE throughout the seasons is obvious. Figure 12b is a histogram of the occurrence of low-frequency scintillations versus the month of the year. It is quite striking that the low-frequency scintillations occur during January, February, March, and April for which months the MUFE is often in the vicinity of 13 Mc/s. However, the MUFE is as low as 13 Mc/s on quite a few occasions also during the months of November and December, yet no low-frequency scintillations were observed. This suggests that while a low MUFE is a necessary condition for the observation of scintillations in the lower octaves it is not a sufficient condition.

Since the MUFE limits the times when scintillations at low frequencies are observed, only those half-hour observing periods in which the MUFE

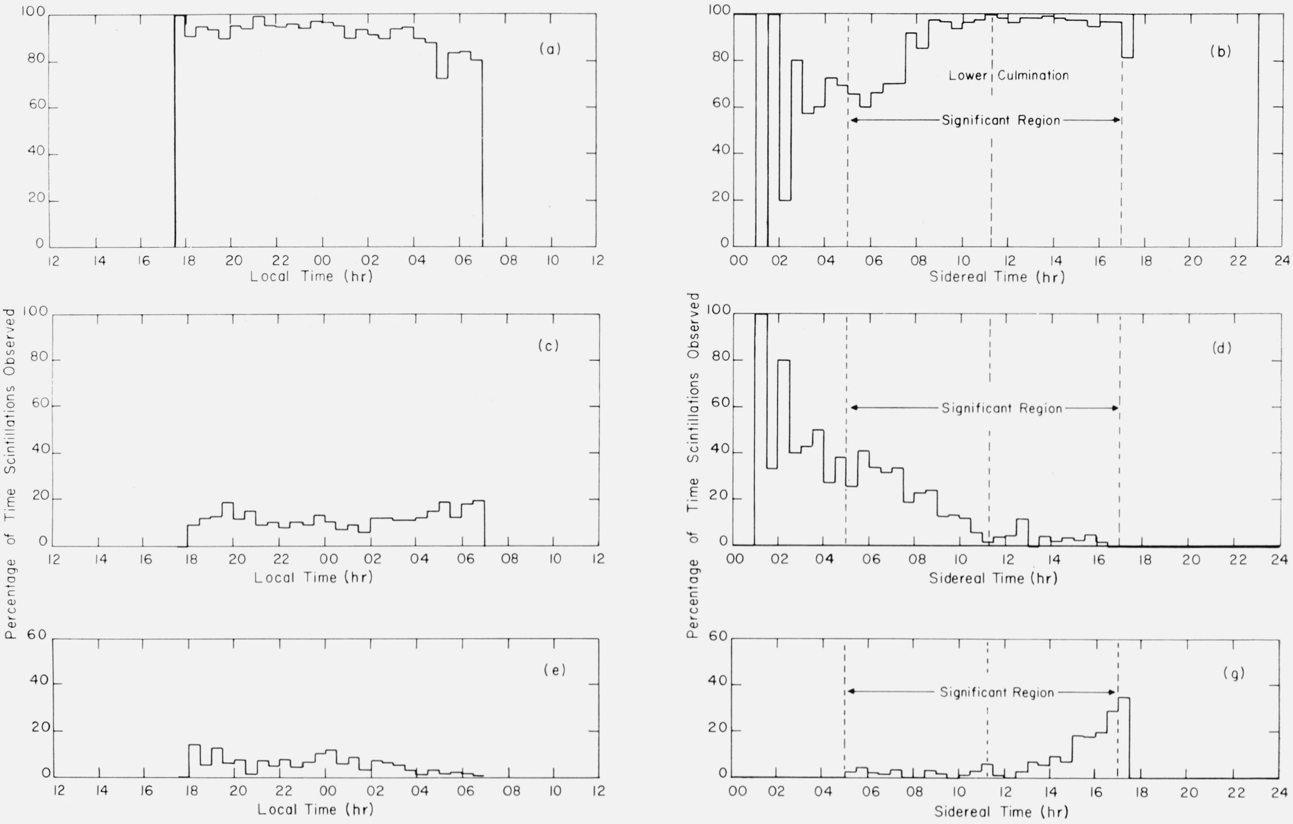

FIGURE 8. *Histograms (a), (c), and (e) represent the local time variations of the percentage occurrence of scintillations which are classified as N, CB_H and CA_H.*

Histograms (b), (d), and (g) are the sidereal time variations of the percentage occurrence of these same three classes of scintillations.

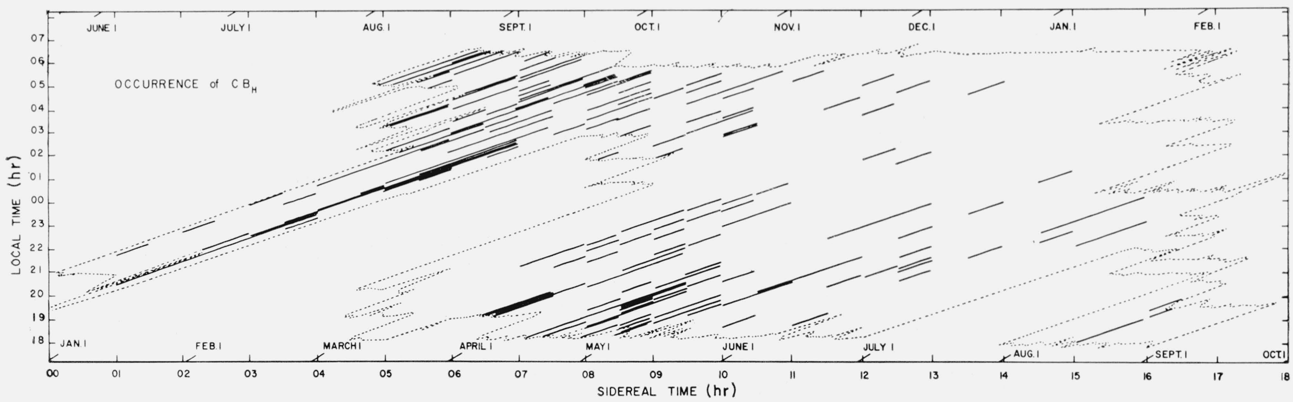

FIGURE 9. *This is a local time versus sidereal time plot of the half-hour observing periods (full lines) in which scintillations classified as CB_H were observed.*

The broken lines enclose the region in which observations were made.

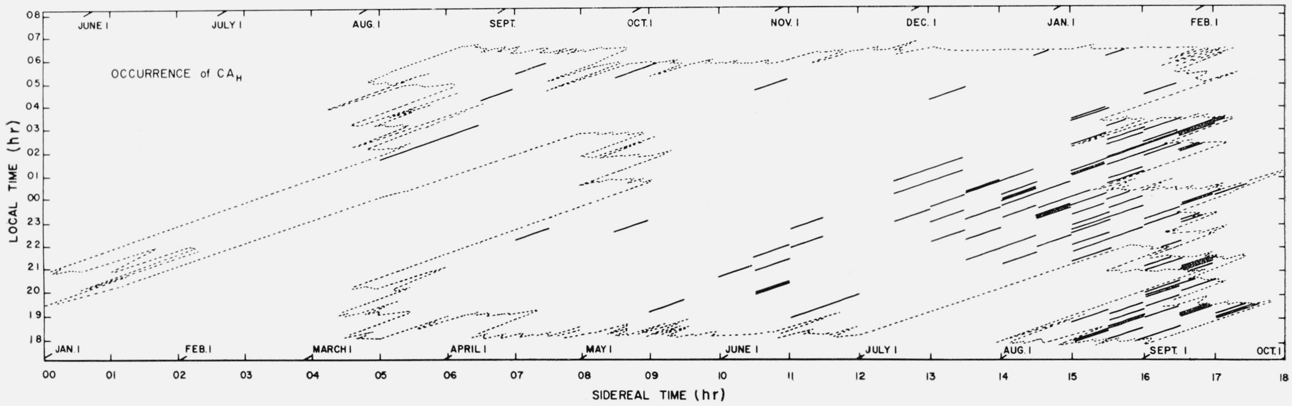

FIGURE 10. *This is local time versus sidereal time plot of the half-hour observing periods (full lines) in which scintillations classified as CA_H were observed.*

The broken lines enclose the region in which observations were made.

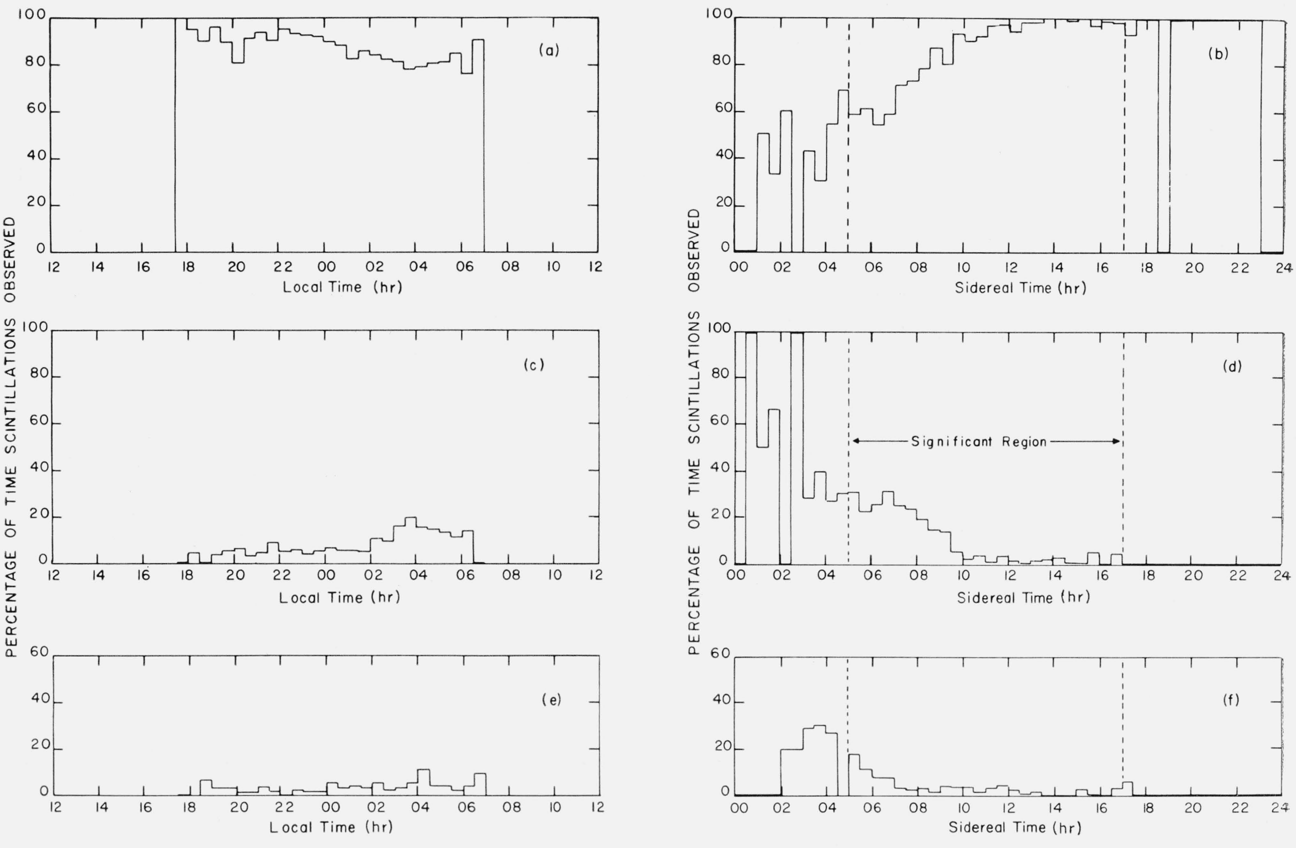

FIGURE 11. *Histograms (a), (c), and (e) represent the local time variations of the percentage occurrence of scintillations which are classified as NC–N/U, NC– and CS–T_L/U and NC– and CS–T_H/U.*

Histograms (b), (d), and (f) are the sidereal time variations of the percentage occurrence of these same three classes of scintillations.

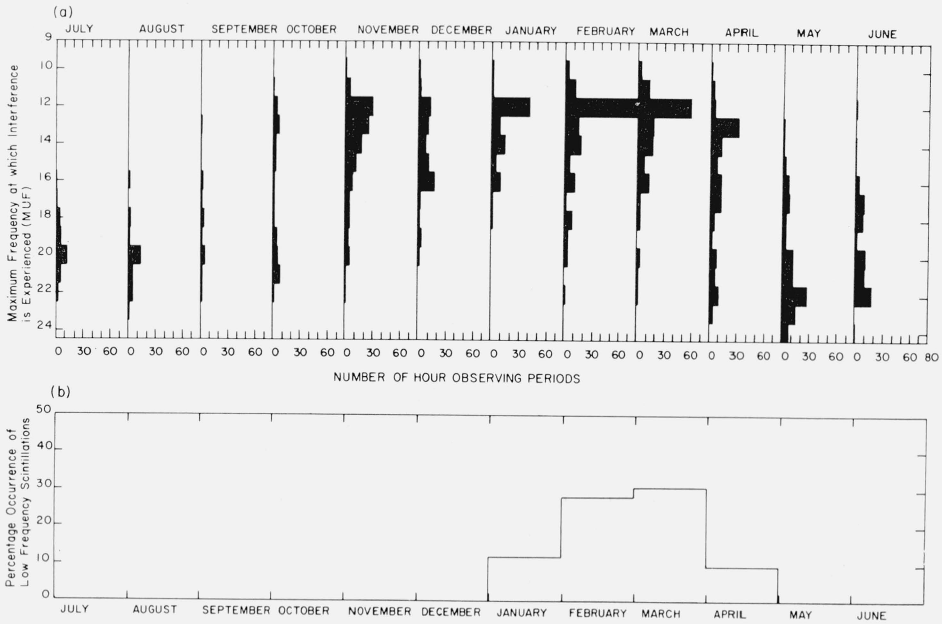

FIGURE 12. *Part (a) is a series of histograms for each month in which the number of hour observing periods is plotted against the MUFE values.*

Part (b) is a histogram of the occurrence of low-frequency scintillations versus the month of the year.

is equal to or less than 15 Mc/s have been used to construct the temporal distributions displayed in figure 13. Figures 13a and 13b represent the local and sidereal time variations of the number of half-hour observing periods in which the MUFE was equal to or below 15 Mc/s, while figures 13c and 13d give the local and sidereal time variations of the percentage occurrence of low-frequency scintillations during these periods. Figure 13a shows that most of the low MUFE values occurred after 0000 hr. Consequently, it is not surprising that the local time distribution of the low-frequency scintillations (fig. 13c) resembles the local time distributions of all scintillations (fig. 5c) only in the post-midnight hours. The strong peak at 2130 hr is perhaps of doubtful significance because of the relatively few half-hour observing periods involved at this local time.

The sidereal time distribution of half-hour observing periods with MUFE$<$15 Mc/s (fig. 13b) is not unlike that for all half-hour observing periods (fig. 6b). Thus it might be expected that the sidereal time distribution of the percentage occurrence of low-frequency scintillations (fig. 13d) would be similar to that for all scintillations (fig. 6d). However, this is not the case. The low-frequency scintillation distribution increases rapidly from zero at 0730 hr to a broad maximum at 1600 hr, whereas the all scintillation distribution increases slowly from 40 percent at 0500 hr and again decreases very slowly to 60 percent at 1700 hr. Consequently, it appears that the low-frequency scintillations occur preferentially between 0730 hr and 1600 hr sidereal time.

4. Broadband Scintillations and Magnetic Activity

Several workers have recognized a connection between magnetic activity and radio-star scintillations. At low geomagnetic latitudes the incidence of scintillations is decreased by increasing magnetic activity [Koster and Wright, 1960] while the reverse is true for higher latitudes [Dagg, 1957]. For all latitudes the scintillation rate increases with magnetic activity [e.g., Booker, 1958].

4.1. Broadband Scintillation Occurrence and Magnetic Activity

In the present investigation a connection between the incidence of scintillations and magnetic activity was sought by correlating the daily percentage occurrence with the magnetic index A_p. During the twelve-month period investigated, only in the months of April, May, June, October, November, and December 1962 and January and February 1963 was there sufficient observing time during each 24 hr to warrant the calculation of a percentage occurrence figure. The correlation coefficients for each of these months together with their 1 and 10 percent significance levels are listed in table 3. It can be seen that the correlation is sometimes positive and sometimes negative, and the coefficients are always below the 10 percent level of significance. Thus no firm association exists between the occurrence of broadband scintillations observed at Boulder and magnetic activity.

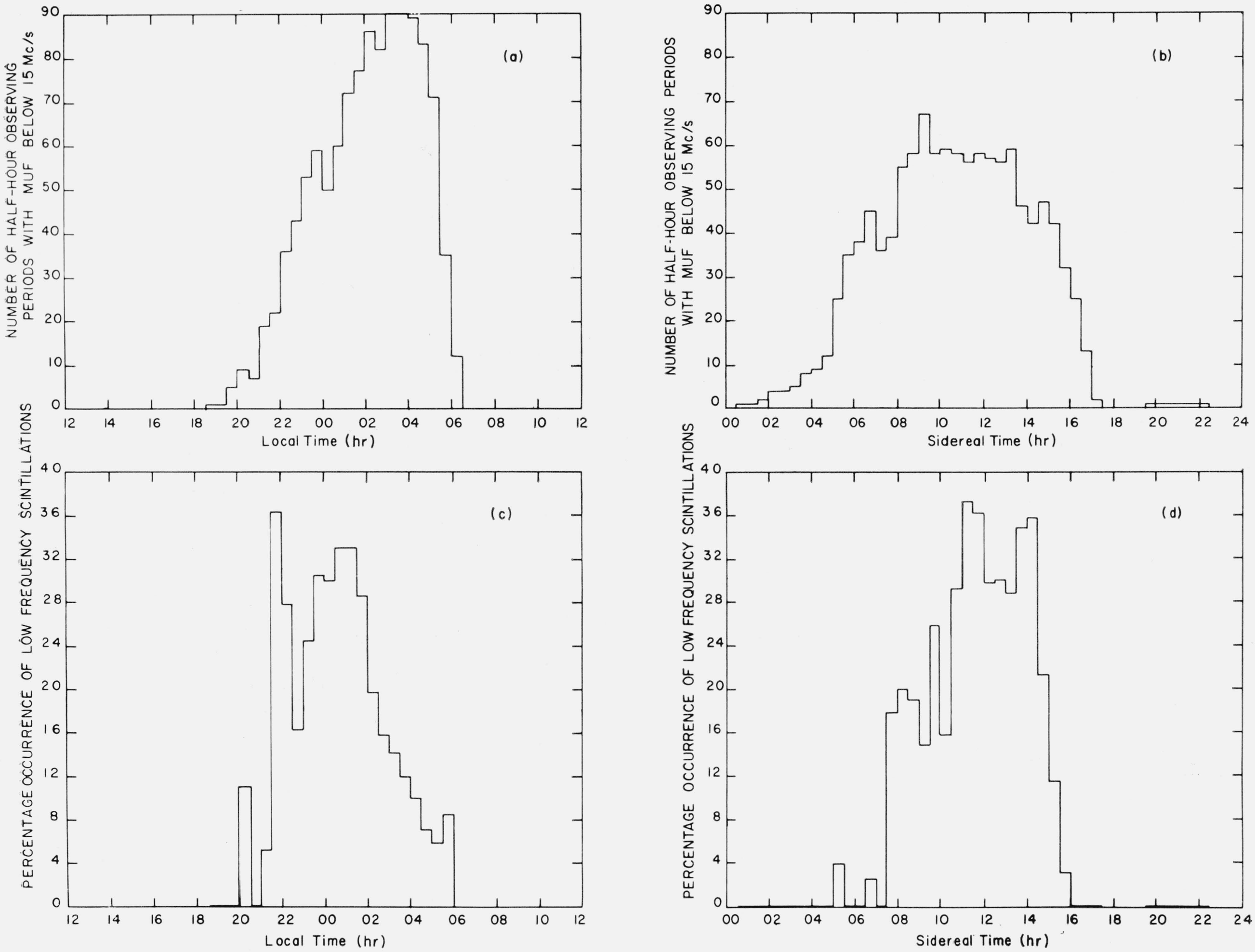

FIGURE 13. *Histograms of the number of half-hour observing periods in which the MUFE was below 15 Mc/s versus (a) local time and (b) sidereal time and histograms of the percentage occurrence of low-frequency scintillations versus (c) local time and (d) sidereal time.*

TABLE 3. *Correlation of scintillation occurrence with magnetic activity* (A_p)

Month	April (1962)	May (1962)	June (1962)	October (1962)	November (1962)	December (1962)	January (1963)	February (1963)
ρ	−0.29	−0.16	0.08	0.02	0.27	0.28	0.11	0.25
1% level	.47	.47	.62	.58	.47	.47	.54	.49
10% level	.31	.31	.43	.39	.31	.31	.36	.32

4.2. Scintillation Rate and Magnetic Activity

When scaling the 12 months spectrograph records being discussed here, each half-hour observing period was labeled according to the quasi-period of any group of scintillations occurring in it. The observing periods were termed fast, slow or very slow according to whether the quasi-period was less than 2 min, between 2 and 10 min or greater than 10 min.

TABLE 4. *Contingency table for scintillation quasi-period versus the* K_p *magnetic index*

K_p \ Quasi-period (T)	$T > 10$ min. (very slow)	10 min. $> T > 2$ min. (slow)	$T < 2$ min. (fast)
0	0 (1)	258 (232)	33 (58)
1	4 (3)	518 (489)	91 (121)
2	4 (4)	625 (604)	129 (150)
3	3 (2)	338 (352)	100 (87)
4	1 (1)	132 (160)	68 (40)
5	0 (1)	34 (61)	43 (15)
6	0 (0)	6 (13)	10 (3)

A contingency table was then constructed for these three classes against the magnetic index K_p. The result is shown in table 4. The numbers in brackets in the various cells of this table represent the number of events expected on the basis of a random distribution. It will be noted that as K_p increases the ratio of the observed to the expected number of events increases for the fast scintillations but decreases for the slow scintillations. This suggests that the quasi-period is not randomly distributed with regard to magnetic activity but rather the quasi-period decreases with increasing magnetic activity. A chi-square test on the data of table 2 shows that the probability that the observed distribution is a random one is less than 1 in 1000.

5. Broadband Scintillations and Ionospheric Conditions

It has long been realized that radio-star scintillations and the ionospheric phenomenon of spread-F [Singleton, 1957] are related and probably have a common origin [Ryle and Hewish, 1950; Little and Maxwell, 1951]. Consequently, associations were sought between broadband scintillations and various properties of the ionosphere.

Figure 14 shows the track of the line of sight from Boulder to Cassiopeia A across the 200, 400, and 600 km levels. Each of the tracks has been divided into 2-hr intervals of sidereal time. The figure also shows the positions of the available bottomside ionosondes. Keeping in mind that the majority of scintillation observations were made in the period 0500 to 1700 hr sidereal time, it is obvious that of the ionosondes available, the one at Winnipeg is the most likely to give information which is representative of the section of the ionosphere through which the Cassiopeia A emissions pass. This is particularly true if attention is limited to the period 1400 to 1700 hr sidereal time. The track through the 200 km level has its closest approach to Winnipeg at 1300 hr, the distance then being 1300 km. At 400 km the closest approach is at 1430 hr, the distance being 800 km, and at 600 km the closest approach is at 1600 hr, the distance being 400 km.

5.1. Scintillations and Absorption

During the scaling of the broadband scintillation data, note was kept of the strength of the scintillations. Each half-hour period in which scintillations were observed was classified according to whether the scintillations were very weak, weak, or strong. These indications for the period 1400 to 1700 hr sidereal time were compared with the incidence of ionospheric blackout as observed at Winnipeg. The results of this comparison appear in the contingency table of table 5. The figures in brackets in the various cells of this table represent the number of events expected on the basis of a random distribution. It will be noted that the no scintillation condition and weak scintillations occur preferentially during

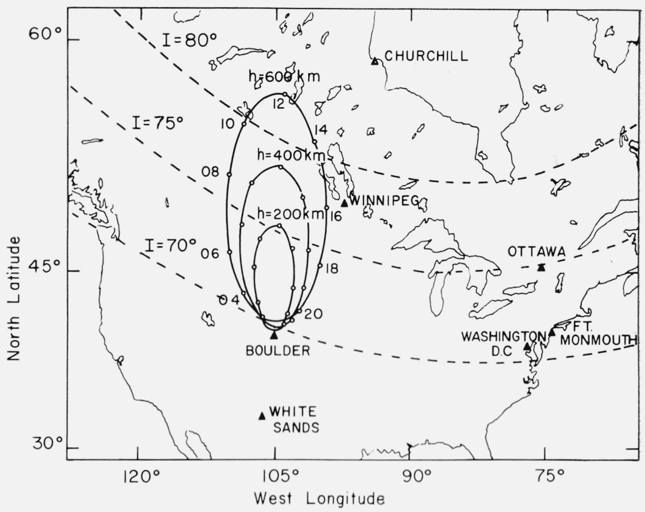

FIGURE 14. *This shows the track of the line of sight from Boulder to Cassiopeia A across the 200, 400, and 600 km levels (full lines).*

Each of the tracks have been divided up into 2-hr intervals of sidereal time. The broken lines represent the 70, 75, and 80° isoclines and the places marked are the locations of ionosondes.

periods of high absorption (blackout), whereas the strong scintillations occur more often than would be expected on a purely random basis when the absorption in the lower ionosphere is low. A chi-square test, based on table 5, shows that the probability that the observed distribution of values in the table is random is less than 1 in 1000. It would appear, therefore, that the strength of the scintillations and indeed their presence or absence depend to some extent on the absorption conditions in the lower ionosphere.

TABLE 5. *Contingency table for scintillation strength versus ionospheric absorption*

	High absorption (blackout)	Low absorption
No scintillation	25 (12)	36 (49)
Very weak Scintillations	3 (3)	13 (13)
Weak Scintillation	24 (22)	91 (93)
Strong Scintillations	10 (25)	121 (106)

5.2. Scintillations and Spread-F

Reference has already been made to the known association between scintillations and spread-F. To demonstrate this association for the present data, the presence or absence of scintillations during each half-hour observing period during the interval of sidereal time 1400 to 1700 hr was compared with the presence or absence of spread-F at Winnipeg at the same time. The result of this comparison is the contingency table of table 6. The figures in brackets in the various cells of this table represent the number of events expected on the basis of a random distribution. The tendency for scintillations and spread-F to be present or absent at the same time will be noted. A chi-square test, based on table 6, shows that the probability that the observed distribution of events in the table is random is less than 1 to 1000.

TABLE 6. *Contingency table for spread-*F *occurrence versus scintillation occurrence*

Scintillations occurring \ Spread-F occurring	NO	YES
NO	22 (7)	14 (29)
YES	30 (45)	201 (186)

It is also instructive to examine the possibility that the severity of the scintillations is related to the severity of the accompanying spread-F. In this comparison the strength of the scintillations was taken as a measure of its severity, whereas the frequency extent (δf) of the spread-F configuration [Singleton, 1962] was used as a measure of its severity. The contingency table resulting from this comparison is shown in table 7. Again the numbers in brackets are the numbers of events expected in the various cells on the basis of a purely random distribution. It will be noted that nowhere is the observed number of events significantly different from the number expected on the basis of a random distribution. Indeed, a chi-square test on this table shows that the probability that the observed distribution is a random one is better than 0.99. It would appear, therefore, that there is little or no association between the severity of scintillations and the associated spread-F.

TABLE 7. *Contingency table for scintillation strength versus the severity of spread-*F (δf_o)

Scintillation strength \ δf_0	0.2	0.3	0.4	0.5	0.6	0.7	0.8
No scintillations	4 (6)	6 (4)	1 (2)	2 (2)	1 (1)	0 (0)	0 (0)
Very weak scintillations	3 (3)	3 (2)	0 (1)	0 (1)	0 (0)	0 (0)	0 (0)
Weak scintillations	31 (31)	19 (20)	10 (9)	8 (8)	3 (4)	2 (1)	2 (2)
Strong scintillations	47 (45)	27 (29)	14 (13)	12 (11)	6 (5)	0 (1)	2 (2)

Warwick [1964] has suggested that the changeover in the fringe pattern of scintillations of the CB_H and CA_H types is the result of the focusing action of the ionospheric lenses which, he suggests, are responsible for the broadband scintillations. The association between the occurrence of spread-F and scintillations suggests that these lenses may be the same ionospheric irregularities as give rise to the spread-F echoes.

The focal length of a lens-type irregularity depends, amongst other things, on its incremental electron density δN. Since the electron density N is proportional to the square of the plasma frequency f_0, δN is proportional to $f_0\delta f_0$. The changeover or focusing frequency (f_m) of CB_H and CA_H scintillation types occurs when the range to the lens equals its focal length [Warwick, 1964]. Therefore, it might be expected that f_m would depend on $f_0\delta f_0$. This possibility has been investigated for CB_H and CA_H scintillations which occur in the sidereal time interval of 1400 to 1700 hr. The f_0 and δf_0 values used were those for the peak of the F-layer at Winnipeg, i.e., f_0 was taken as the critical frequency of the F-layer and δf_0 as the spread in critical frequency associated with the accompanying spread-F configuration. Figure 15 is the scatter diagram which results when $\log f_m$ is plotted against $\log (f_0\delta f_0)$. This scatter has a correlation coefficient of 0.48 which is significant at the 1 percent level (0.42). The line of best fit to the scatter is

$$\log f_m = 0.43 \log (f_o\delta f_0) + 1.543.$$

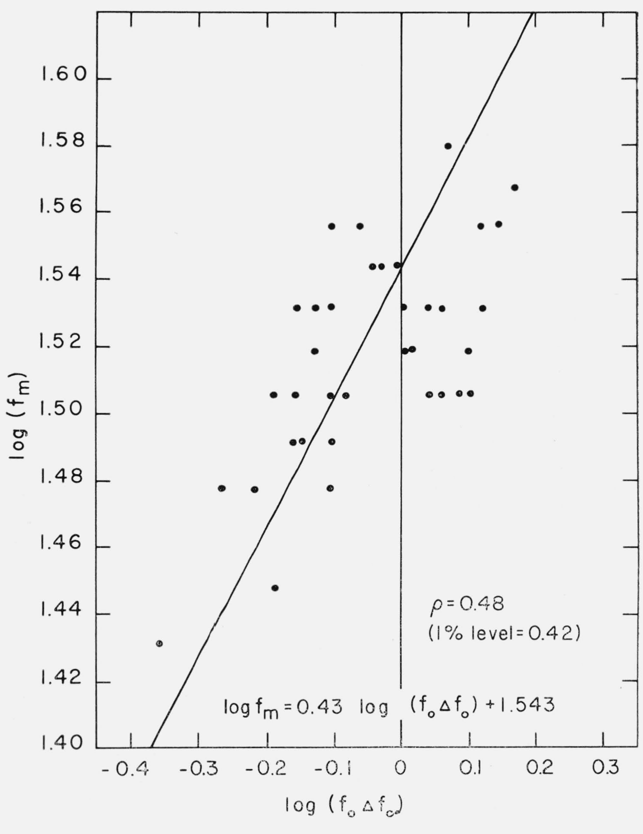

FIGURE 15. *This is the scatter which results when the logarithm of the focusing frequency* (f_m) *is plotted against the logarithm of the product of the* F*-layer critical frequency* (f_0) *and the frequency extent of the spread-*F *configuration* (δf_0).
The line which best fits the scatter is also shown.

This suggests that f_m^2 is proportional to $f_0 \delta f_0$, the constant of proportionality being in the vicinity of 1.2×10^3. Thus broadband scintillations, besides occurring at the same time as spread-F, are related in a simple way, through their focusing frequency, to the parameters of the spread-F configuration.

6. Conclusions

The main conclusion to be drawn from this statistical investigation of 12 months observations of the scintillations of Cassiopeia A made with the Boulder spectrointerferometer are as follows.

(1) The scintillations observed are broadband centered anywhere in the frequency range of 7.6 to 41 Mc/s. Bandwidths of 2:1 are common. However, bandwidths as high as 4:1 are encountered very rarely.

(2) The occurrence pattern of the scintillations, while varying little with season, is markedly dependent on local and sidereal time. The local time variation has a broad maximum centered on 0100, while the sidereal time variation peaks some 2 to 3 hr on either side of a minimum at the time of lower culmination.

(3) Besides involving changes in signal strength some scintillations are associated with changes in the apparent position of the source. There are two main position shift configurations which are mirror images of each other. Each of these configurations implies an initial sudden shift in the apparent position of the source followed by a gradual recovery to and overshoot of the original source position and a final sudden shift back to the undisturbed position of the source. The sense of the initial shift, recovery, etc., reverses as frequency is increased, there being an intermediate frequency at which there is apparently no position shift. Scintillations associated with position shifts while occurring with equal likelihood at any local time have an occurrence pattern which is markedly dependent on sidereal time. The CB_H type occurs mainly before 1200 hr sidereal time, while the CA_H type occurs mainly after this time.

(4) Most scintillations are free from dispersion. However, for some scintillations the low frequencies are delayed relative to the high, while for others the reverse is the case. Dispersion occurs for sidereal times earlier than 0900 hr and local times later than 0200 hr.

(5) The occurrence of scintillations does not correlate with magnetic activity. However, the quasi-period of groups of scintillations is found to decrease as magnetic activity increases.

(6) The occurrence of scintillations correlates positively with the occurrence of spread-F as observed on a nearby ionosonde. The severity of the scintillations, however, does not seem to be related to the severity of the associated spread-F. The focusing frequency of the scintillations which exhibit position shifts is found to be related in a simple way to the parameters of the associated spread-F configuration.

Part II of this series will consider the extent to which these observations can be explained by the refractive properties of the ionospheric irregularities which are believed to give rise to the broadband scintillations.

It is with pleasure that the author acknowledges the use of the facilities afforded him by the High Altitude Observatory to carry out the work reported here while on sabbatical leave from the University of Queensland. In particular, he would like to thank Dr. James W. Warwick of the Observatory staff who suggested the investigation and maintained a very active interest in it.

The research reported here was sponsored, in part, by the Air Force Cambridge Research Laboratories.

7. References

Aarons, J. (1963), Radio Astronomical and Satellite Studies of the Atmosphere (North-Holland Pub. Co., Amsterdam).

Boischot, A., R. H. Lee, and J. W. Warwick (1960), Low-frequency solar bursts and noise storms, Astrophys. J. **131,** 61–74.

Bolton, J. G., and G. J. Stanley (1948), Observations on the variable source of cosmic radio frequency radiation in the constellation of Cygnus, Australian J. Sci. Res. **1A,** 58–69.

Booker, H. G. (1958), The use of radio stars to study irregular refractions of radio waves in the ionosphere, Proc. IRE **46,** 298–314.

Burrows, K., and C. G. Little (1952), Simultaneous observations of radio star scintillations on two widely spaced frequencies, Jodrell Bank Annals **1,** 29–35.

Chivers, H. J. A. (1960), The simultaneous observations of radio star scintillations of different radio-frequencies, J. Atmospheric Terrest. Phys. **17,** 181–187.

Dagg, M. (1957), The correlation of radio-star-scintillation phenomena with geomagnetic disturbances and the mechanism of motion of the ionospheric irregularities in the F region, J. Atmospheric Terrest. Phys. **10,** 194–203.

Koster, J. R., and R. W. Wright (1960), Scintillation, spread F and transequatorial scatter, J. Geophys. Res. **65,** 2303–2306.

Lee, R. H., and J. W. Warwick (1964), A spectrographic interferometer, Radio Sci. J. Res. NBS/USNC–URSI **68D,** No. 7, 807–811.

Little, C. G., and A. Maxwell (1951), Fluctuations in the intensity of radio waves from galactic sources, Phil. Mag. **42,** 267–278.

Ryle, M., and A. Hewish (1950), The effects of the terrestrial ionosphere on the radio waves from discrete sources in the galaxy, Monthly Not. Roy. Astrom. Soc. **110,** 381–394.

Singleton, D. G. (1957), A study of "spread-F" ionosphere echoes at night at Brisbane, III. Frequency spreading, Australian J. Phys. **10,** 60–76.

Singleton, D. G. (1962), Spread-F and the perturbations of the maximum electron density of the F layer, Australian J. Phys. **15,** 242–260.

Smith, F. G. (1950), Origin of the fluctuations in the intensity of radio waves from galactic sources, Nature **165,** 422–423.

Warwick, J. W. (1961), Theory of Jupiter's decametric emission, Annals New York Academy of Sciences **95,** 39–60.

Warwick, J. W. (1963), Dynamic spectra of Jupiter's decametric emission, 1961, Astrophys. J. 137, 41–60.

Warwick, J. W. (1964), Radio-star scintillations from ionospheric waves, Radio Sci. J. Res. NBS/USNC–URSI **68D,** No. 2, 179–188.

Wild, J. P., and J. A. Roberts (1956), The spectrum of radio-star scintillations and the nature of inequalities in the ionosphere, J. Atmospheric Terrest. Phys. **8,** 55–75.

(Paper 68D8–385)